ELSEVIER

Journal of Fluids and Structures 19 (2004) 141–158

JOURNAL OF FLUIDS AND STRUCTURES

www.elsevier.nl/locate/jnlabr/yjfls

Effects of free-end corner shape on flow structure around a finite cylinder

C.W. Park[a], S.J. Lee[b,*]

[a] School of Mechanical Engineering, Kyungpook National University, Daegu 702-701, South Korea
[b] Department of Mechanical Engineering, Pohang University of Science and Technology, Pohang 790-784, South Korea

Received 15 January 2003; accepted 27 November 2003

Abstract

The flow structure around the free end of a finite circular cylinder embedded in an atmospheric boundary layer (ABL) over open terrain was investigated experimentally by modifying the free-end corner shape. The experiments were carried out in a closed-return subsonic wind tunnel. A finite cylinder (FC) with an aspect ratio (height/diameter) of 6 was mounted vertically on a long flat plate. The velocity fields near the FC free end were measured using the single-frame double-exposure PIV (particle image velocimetry) method. The Reynolds number based on cylinder diameter for the PIV measurements was about $Re = 7500$. A hot-wire anemometer was employed to analyze the spectral characteristics of the wake structure. As a result, for the FC with a right-angled flat-tip free end, there is a strong vortical structure showing counter-rotating twin vortices near the FC free end. It is caused by the interaction between the entrained ambient fluids from both sides of the FC and the downwash flow from the FC free end. Due to the descending separated shear flow from the FC free end, regular vortex shedding from the cylinder seems to be suppressed and the vortex formation region is barely noticeable in the region near the FC free end, irrespective of free-end edge shape. For the case of the flat-tip free-end FC, the separated shear flow has a stronger downwash compared to the radiussed-tip free-end FC, reducing the size of the recirculation bubble in the near-wake region.

Keywords: Finite cylinder (FC); Free end; Particle image velocimetry (PIV); Wake structure

1. Introduction

A circular cylinder has been regarded as a representative bluff body showing a two-dimensional flow structure in its wake. Many studies of the flow around a circular cylinder have been carried out because of its simple geometry and coherent vortex structure. However, the wake behind a two-dimensional (2-D) bluff body placed in a uniform flow is rarely two dimensional in the strict sense, even at low Reynolds numbers at which the vortex street is formed. The three dimensionality of the cylinder wake has been often characterized by flow phenomena such as slantwise shedding, irregular waviness and bowed vortices. The three-dimensional (3-D) flow characteristics are usually enhanced by with increasing Reynolds number (Slaouti and Gerrard, 1981; Williamson, 1989).

In the near-wake region just behind a 2-D cylinder, however, the three dimensionality of the wake is weak because the vortex shedding is regular and parallel to the cylinder axis. Therefore, the cylinder wake has been assumed to be 2-D in view of its coherent structure, in which the Strouhal number is constant along the cylinder axis when appropriate end plates are attached (Szepessy and Bearman, 1992). Williamson (1989) found a discontinuity in the Strouhal and

*Corresponding author. Tel.: +82-54-279-2169; fax: +82-54-279-3199.
E-mail address: sjlee@postech.ac.kr (S.J. Lee).

0889-9746/$ - see front matter © 2003 Elsevier Ltd. All rights reserved.
doi:10.1016/j.jfluidstructs.2003.12.001

Reynolds number relationship at low Reynolds numbers due to the transition from one oblique vortex shedding mode to another. He mentioned that the critical Reynolds number depended on the flow nonuniformity, end conditions, and the level of free-stream turbulence.

Many high-rise tall buildings can be simplified to a finite cylinder (hereafter, denoted as FC) with a free end. The study of finite-span bluff bodies located in an atmospheric boundary layer (hereafter, denoted as ABL) is of interest due to its practical importance in civil and wind engineering applications (Uematsu et al., 1990; Fox et al., 1993). The presence of a free end modifies the flow structures in the near-wake region, such as the vortex structure, vortex shedding pattern, turbulent structure and surface pressure distribution.

The three dimensionality of the cylinder wake is caused by many factors such as nonuniformity of the free-stream flow, variation of longitudinal secondary vortices, and low aspect ratio of the cylinder. In particular, the FC free end is the major cause of the three dimensionality of the cylinder wake. Therefore, in order to properly design high-rise structures such as tall buildings and cooling towers, the wind loading and flow structure should be considered at the design process. An example is the recirculation flow behind a chimney located on the ship deck, where the dispersion of contaminant emitted by the chimney is substantially affected by its free-end shape.

Baban and So (1991) mentioned that the unsteady drag was caused by the fluctuating recirculation flow formed behind the FC free end. Okamoto and Sunabashiri (1992) found that the wake behind FCs of small aspect ratio ($L/D = 1-2$) is symmetric, but that the wake pattern becomes three dimensional when the aspect ratio exceeds $L/D = 4$. Farivar (1981) investigated the effect of FC free end on the mean pressure, pressure fluctuations and drag force acting on FC of various aspect ratios exposed to a uniform flow. Regular vortex shedding disappeared for aspect ratios smaller than $L/D = 7.5$.

Kareem and Cheng (1999) investigated the pressure and drag fluctuations for FCs located in a simulated boundary layer. The lateral velocity fluctuations due to strong turbulence intensity of approaching shear flow made a large contribution to the pressure fluctuations, however, the contribution of vortex shedding from the FC was weak. Kahraman et al. (2002) tried to control the vortex formation from a vertical cylinder in shallow water using roughness elements located on the bottom surface. They employed a PIV (particle image velocimetry) velocity measurement technique to obtain global and instantaneous flow patterns.

Most previous studies have dealt with FCs located in a uniform flow. However, the flow structure behind a FC embedded in an ABL has not been fully investigated. In our previous studies (Park and Lee, 2000, 2002), we found that the flow past the FC free end had a complicated 3-D wake structure that was quite different from that of 2-D cylinder, due to the downwash from the flow separated over the FC free end.

The finite cylinder with the right-angled flat-tip free end has been most commonly studied. However, many bluff bodies have various free-end shapes. From an aerodynamic point of view, it is important to know the effects of different free-end shapes on the wake structure near the FC free end. Therefore, the main objective of this study was to investigate the flow structure near the various free ends of the FC embedded in an ABL. The free-end corner shape was systematically varied and flow analysis was carried out using the PIV technique, flow visualization and hot-wire anemometry. In the end, the results of this study can serve as the basic data for the design process of high-rise building or chimney tip shapes and other relevant CFD analysis.

2. Experimental apparatus and methods

2.1. Hot-wire anemometry and flow visualization

The experiments were performed in a closed-return subsonic wind tunnel with a test-section of (width × height × length) = (0.72 m × 0.6 m × 6 m). To generate a neutrally buoyant ABL, spires and an artificial lawn were installed on the upstream side of a long flat plate, 57 mm above the bottom of the test-section. The reference velocity was fixed at $U_0 = 10$ m/s at the FC free end and the corresponding Reynolds number based on the cylinder diameter ($D = 30$ mm) was about $\mathrm{Re} = 20\,000$. The FC model was installed vertically, 3.9 m downstream of the leading edge of the flat plate. A schematic diagram of the wind tunnel test-section and measurement system is given in Fig. 1. The FC model used in this study was made of stainless steel. In order to investigate the effects of FC free-end corner shape on the wake structure, we made four different FC free-end shapes: flat, bevelled, radiussed and hemispherical tips. The free-end shapes and dimensions of the FC models tested in this study are shown in Fig. 2.

The velocity profiles of the simulated ABL were measured using a hot-wire anemometer. The mean velocity and turbulence intensity profiles of the streamwise velocity component measured at the location of FC model ($X = 0$) are

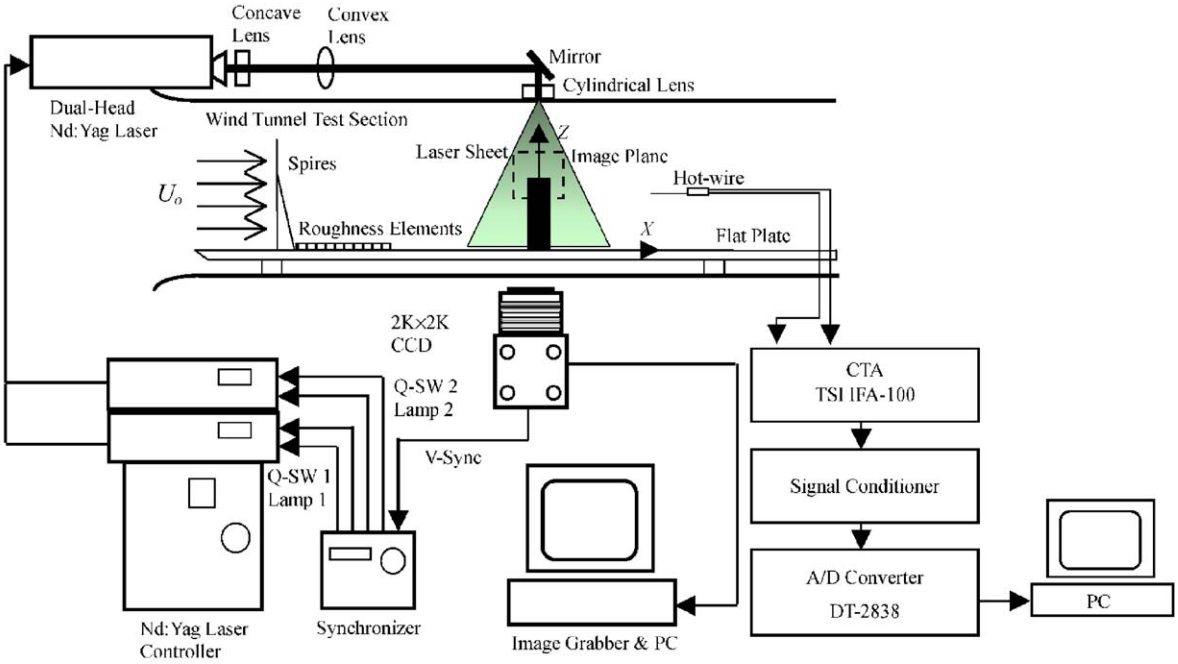

Fig. 1. Wind tunnel test-section and measurement system.

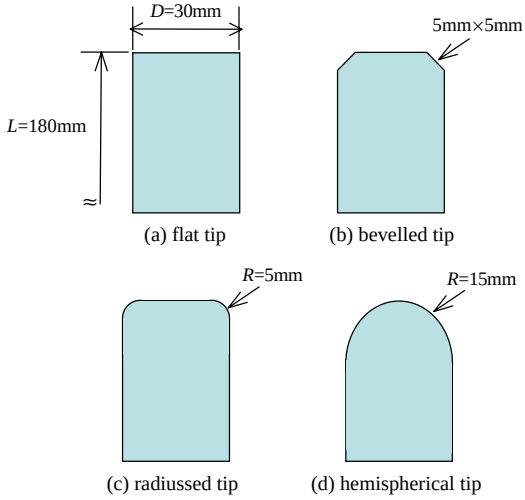

Fig. 2. Free-end shapes of the four FC models tested in this study: (a) flat tip; (b) bevelled tip; (c) radiussed tip; and (d) hemispherical tip.

shown in Fig. 3. The mean streamwise velocity profile in the ABL follows a power law of the form:

$$U(Z)/U_0 = (Z/L)^n, \tag{1}$$

where U_0 is the reference velocity and L is the FC height. The velocity profile was well fitted by $n = 0.14$, corresponding to an ABL over open terrain (Simiu and Scanlan, 1996).

In this kind of wind engineering experiment, the simulated ABL should reproduce not only the mean velocity and turbulence intensity profiles, but also the power spectrum of the streamwise velocity component (Park and Lee, 2002; Simiu and Scanlan, 1996). Fig. 4 shows the power spectral density (PSD) distribution of the longitudinal velocity component of the oncoming ABL over open terrain at the height of $Z = 0.25$ m. The integral length scale (L_u^x)

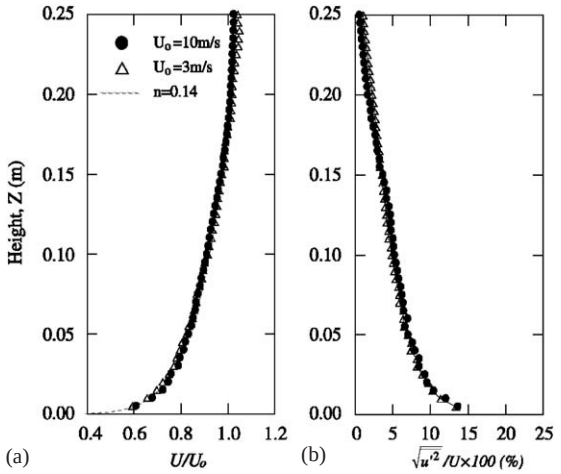

Fig. 3. Streamwise mean velocity and turbulence intensity profiles measured at the FC location ($X = 0$): (a) mean velocity and (b) turbulence intensity.

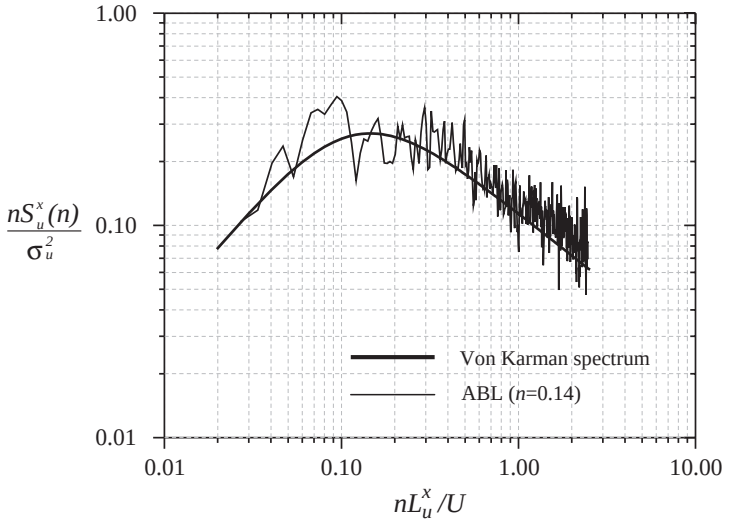

Fig. 4. Power spectral density of streamwise velocity component at $Z = 0.25$ m ($U_0 = 10$ m/s).

of the oncoming ABL flow was estimated by calculating the autocorrelation of the streamwise velocity fluctuations, assuming Taylor's hypothesis. The integral length scale ranged from 32 to 59 cm and the power spectral density distribution of the oncoming flow velocity at the reference height of $Z = 0.25$ m was well matched with the von Kármán spectrum given below:

$$\frac{nS_u(z,n)}{\sigma_u^2} = 4\frac{nL_u^x}{\bar{U}} \Big/ \left[1 + 70.8\left(\frac{nL_u^x}{\bar{U}}\right)^2\right]^{5/6}, \tag{2}$$

where $S_u(z,n)$ is the PSD distribution of streamwise velocity at frequency n, and σ_u is the r.m.s. (root mean square) value of fluctuation of the streamwise velocity component u. This indicates that the ABL simulated in the wind tunnel test-section is kinematically similar to the full-scale natural wind characteristics.

The aspect ratio defined as the ratio of the height L to the diameter D of FC model was set to $L/D = 6$. In order to avoid flow-induced structural vibrations, the natural frequency of the FC model was set to be greater than 20 times the

vortex shedding frequency (Baban and So, 1991). A horseshoe vortex can be formed at the junction of the FC model and the ground plate. However, since the present study focused on the flow near the FC free end and all measurements were performed in the region between mid-height and the free end of FC model, the effects of the horseshoe vortex were assumed insignificant (Okamoto and Sunabashiri, 1992).

The flow velocity was measured using an I-type hot-wire probe connected to a constant temperature hot-wire anemometer (TSI IFA 100). The hot-wire probe was moved using a 3-D traverse with an accuracy of 10 μm. At each measurement location, 32 000 samples were acquired at a sampling rate of 2 kHz, after low-pass filtering at 800 Hz. During the experiments, the temperature variation in the wind tunnel test-section was maintained not to exceed 0.5°C. West and Apelt (1982) mentioned that the Strouhal number is independent of blockage ratio and cylinder aspect ratio for blockage ratios less than 6%. Since the maximum blockage ratio of the tested FC models was about 1.38%, the blockage effects were considered to be insignificant.

To visualize the flow around the FC free end, a particle tracer method was employed in a circulating water channel with test-section of (width × height × length) = (0.3 m × 0.2 m × 1.2 m). The free-stream velocity was fixed at 12 cm/s and nearly the same ABL as that for the wind tunnel tests was simulated in the water channel. Polyvinylchloride particles of average diameter of 100 μm were seeded as tracer particles. The particle pathlines were illuminated with a thin cold light sheet emitted from a 150 W halogen lamp. The scattering particle images were photographed with a digital camera (Olympus C-3030).

2.2. Particle image velocimetry (PIV)

The entire flow field around a FC model is usually not easy to measure with point-wise velocity measuring instruments, such as hot-wire anemometers or laser Doppler velocimeters (LDV). In addition, conventional flow visualization methods give only qualitative flow information. Due to rapid advances in computers, optics and digital image processing techniques, instantaneous velocity fields can be extracted using a specially implemented PIV technique. The PIV method has been regarded as a reliable velocity field measurement technique (Adrian, 1991).

In the present study, the single-frame double-exposure PIV technique was employed to quantitatively measure the velocity fields near the FC free end. Due to limitations of the image size and consideration of proper interrogation window size, the reference velocity was fixed at $U_0 = 3$ m/s and the corresponding Reynolds number based on the cylinder diameter was about Re = 7500. The experimental set-up for the single-frame PIV velocity field measurements was shown in Fig. 1.

The PIV system consists of a high-resolution CCD camera, a dual-head Nd:Yag laser, a frame grabber, a synchronizing device and a computer. The high-resolution CCD camera (SMD 4M4) with a spatial resolution of 2K × 2K pixels was used to capture particle images. The 12-bit air-cooled CCD camera can capture 4 images per second at a 100% fill factor. The maximum energy of the two-head Nd:Yag laser is about 100 mJ per pulse. The CCD camera and Nd:Yag laser were synchronized using a delay generator. For the single-frame PIV measurements, two successive particle images were recorded on a single frame. The CCD camera used in this study has a special built-in image-shifting feature that is ideal for resolving the directional ambiguity problem encountered in conventional single-frame PIV methods.

During the first exposure of the CCD camera, the particle image scattered by the first laser pulse is recorded on the CCD sensor array. The CCD sensor array is then translated by prescribed pixel lines within the time interval Δt, and starts the second exposure to capture the second particle image. In this experiment, the second particle image was shifted 9 pixels by translating the CCD sensor array and the time interval between two laser pulses was set to be $\Delta t = 70-100$ μs, depending on the experimental condition. The two particle images are superimposed on a single-frame and the double-exposed single-frame image is then cross-correlated to extract the instantaneous velocity field. Small olive oil droplets of 1–3 μm in diameter were used as seeding tracers. To generate tracer particles, compressed air was supplied to olive oil through a Laskin nozzle having several fine holes.

A thin laser light sheet was formed by passing the laser beam through a mirror and through spherical and cylindrical lenses. The CCD camera was installed perpendicular to the laser light sheet to capture the scattered particle images of the investigated flow. Details of the single-frame PIV method including measurement accuracy were described in Shin et al. (2000). In this study, the fields of view around the FC model were 8 cm × 8 cm in size for the vertical XZ-plane measurements and 11 cm × 11 cm for the horizontal XY-plane measurements. The interrogation window size was 64 × 64 pixels and overlapped 50%.

To obtain the time-averaged mean flow structure, 350 instantaneous velocity fields were obtained for each free-end shape. These instantaneous velocity fields were ensemble averaged to obtain spatial distributions of the mean velocity and turbulence statistics. The turbulent kinetic energy (TKE) was calculated using the following 2-D approximation

with the assumption of isotropic flow structure:

$$\tfrac{1}{2}q^2 = \tfrac{1}{2}(\overline{u'^2} + \overline{v'^2} + \overline{w'^2}) \approx \tfrac{3}{4}(\overline{u'^2} + \overline{v'^2}). \tag{3}$$

Therefore, the true TKE will be a little different from the present results in the region where the isotropic assumption is not fulfilled.

3. Results and discussion

3.1. Flow visualization

Flow around the FC free end was visualized using a particle tracer method in a circulating water channel. Fig. 5 shows the visualized flow in the vertical XZ-plane passing through the wake center-line ($Y/D = 0$). The oncoming flow moves upward and accelerates near the forward free end, then separates from the circumference of the FC free end. When the FC free end is beveled or radiussed, however, the size of the recirculation bubble above the FC top decreases, compared to the flat tip, due to the more streamlined free-end shape. In the central wake plane, the separated shear layer reattaches to the cylinder tip just ahead of the rear edge, except for the case of the hemispherical tip shown in Fig. 5(d). After passing the FC free end, the separated shear layer moves downward in all cases toward the FC mid-span and forms a large recirculating flow rotating in a clockwise sense.

Fig. 6 shows top views of the flow near the free end in the horizontal XY-plane at the height of $Z/L = 0.9$. The flow in the central wake region is mainly governed by the interaction between the inclined shear layer from the FC free end and the flow entrained from both sides of the FC. The wake structure is nearly symmetric with respect to the central section ($Y/D = 0$) of the wake, irrespective of the FC free-end shape. For the right-angled flat-tip FC (Fig. 6(a)), the visualized flow shows the general double recirculation region usually formed behind a 2-D cylinder. In the cases of the modified FC (Figs. 6(b)–(d)), the size of the wake region is reduced and the wake center-line velocity seems to be faster, compared to the FC with flat-tip free end. The modification of sharp-edged FC tip shape can reduce the width of wake formed behind the FC.

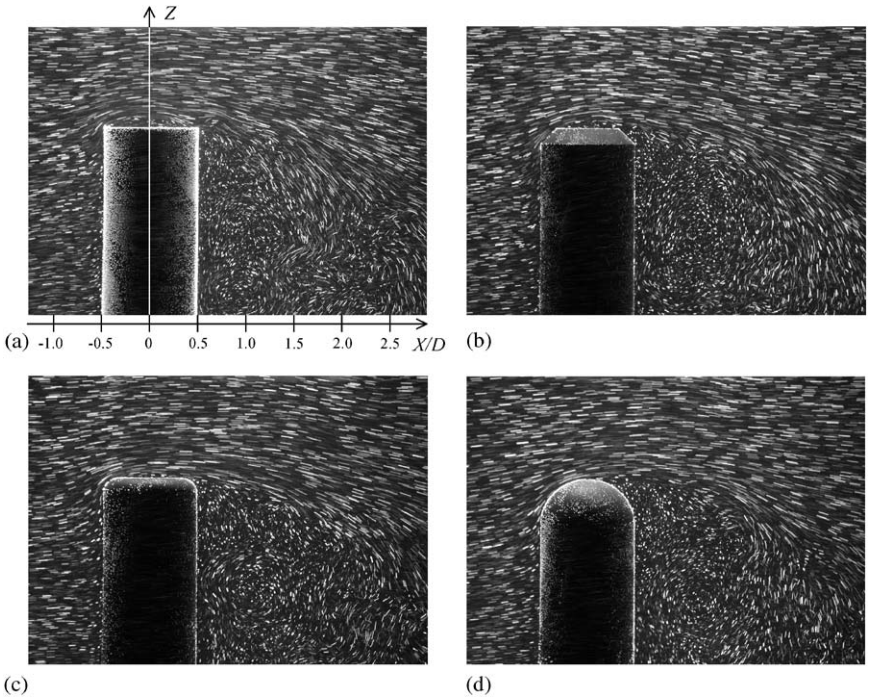

Fig. 5. Visualized flow around the FC free end in the vertical XZ-plane at $Y/D = 0$: (a) flat tip; (b) bevelled tip; (c) radiussed tip; (d) hemispherical tip.

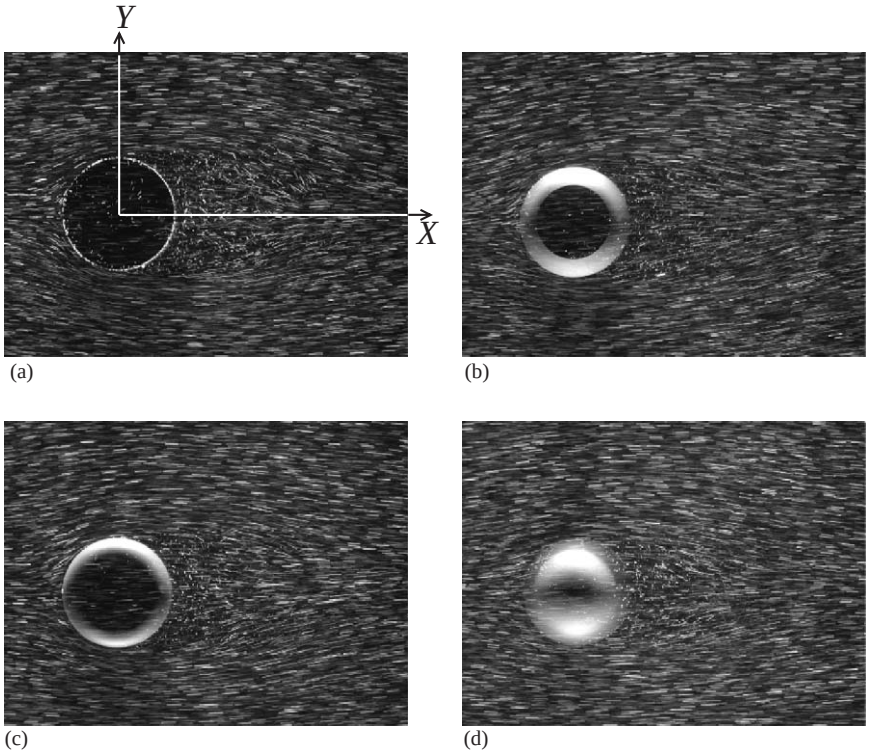

Fig. 6. Top view of visualized flow in horizontal XY-plane at $Z/L = 0.9$: (a) flat tip; (b) bevelled tip; (c) radiussed tip; and (d) hemispherical tip.

Fig. 7 represents the visualized flows in the vertical cross-section (YZ-plane) at a downstreamwise location of $X/D = 0.3$ for four different FC free-end shapes. The flow field was photographed from a downstream location. For the case of flat-tip FC, the oncoming flow begins to roll-up from the cylinder circumference and forms a counter-rotating vortex pair as shown in Fig. 7(a). The left and right vortices rotate in the clockwise and the counter-clockwise sense, respectively. The two vortices are almost symmetric, but differ slightly in size. This kind of vortical flow structure was not observed for the other FC models.

3.2. Vortex shedding frequency and formation length

The velocity time series acquired in the FC wake were analyzed to investigate the effect of the FC free-end shape on the vortex shedding frequency (f_s). For a 2-D circular cylinder, the large-scale vortices shed from the two sides of the cylinder are almost uniform along the cylinder spanwise direction. However, the wake behind a FC with a free end is quite different from the wake behind a 2-D cylinder having the same diameter. In particular, the regular vortex shedding on the 3-D cylinder is influenced by the downwash separated flow from the FC free end. The separated shear flow affects the wake structure over most of the FC.

Fig. 8 shows the power spectral density (PSD) distributions measured at the downstream location $X/D = 3$, $Y/D = 2.0$ and $Z/L = 0.5$ for the four FC free-end shapes. The vortex shedding frequencies for the FCs are lower than that for a 2-D cylinder ($f_s = 66$ Hz) at the same flow speed in uniform flow. The decrease of the vortex shedding frequency seems to be related to the influx of ambient flow into the wake region due to the descending flow. Since the PSD distribution was measured at the mid-height of the cylinder, the effects of the wall boundary layer and horseshoe vortex near the ground plate on the vortex shedding frequency can be assumed to be negligible, although the root effect may go many diameters upward. Among the four free-end shapes tested in this study, the FC free end with the bevelled tip has the smallest peak frequency of 45 Hz, and the right-angled flat-tip FC has the largest value of 47 Hz. The difference in peak frequency is not so large amongst the modified tips tested in this study.

Regarding the wind loads of the cylinder, the attenuation of the vortex shedding frequency of the FC can affect the low frequency characteristics and is more or less important in the drag or lift measurement. However, the turbulent flow

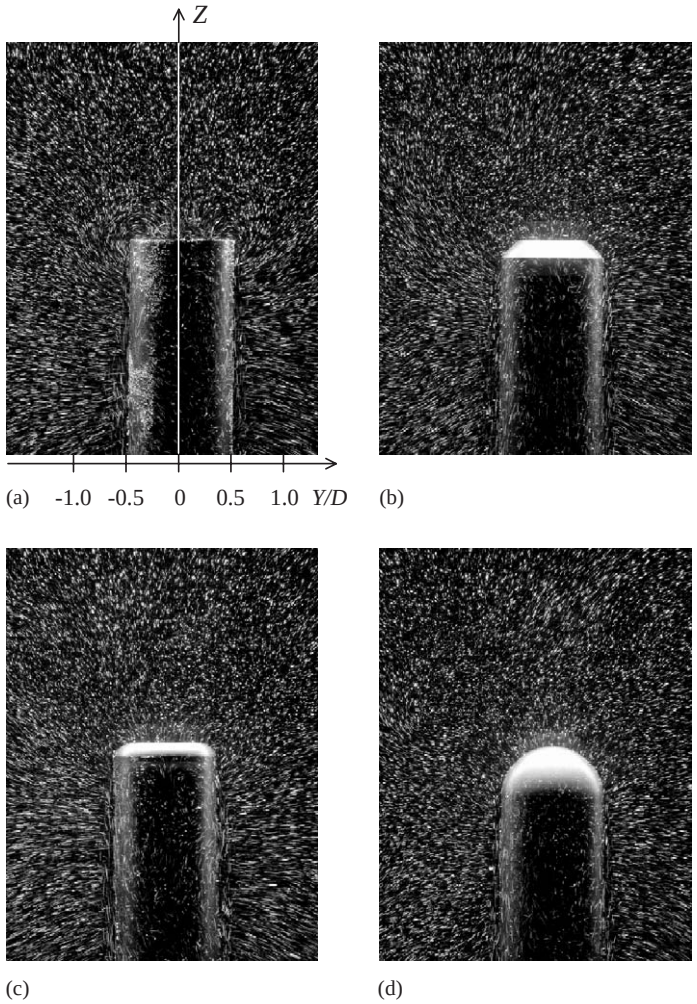

Fig. 7. Cross-sectional view of flow around the FC free end in YZ-plane at $X/D = 0.3$: (a) flat tip; (b) bevelled tip; (c) radiussed tip; and (d) hemispherical tip.

field induced by the separated shear flow from the FC free end may also be the major cause of the induced oscillation or vibration on the cylinder. Baban and So (1991) mentioned that the drag force fluctuations were increased due to the highly turbulent recirculation flow in the wake region, and this was attributed to the unsteady turbulent shear flow separated from the free end of the FC. Consequently, in addition to the vortex shedding characteristics, the flow field analysis around the FC including the turbulence statistics is needed and is discussed in detail in the next velocity-field-measurement sections.

The entrainment of ambient fluid into the wake region affects not only the wake structure but also the vortex formation region formed behind the FC, as shown in Fig. 9. A single hot-wire probe was used to measure the length of the vortex formation region. The streamwise velocity was measured along the wake center-line ($Y/D = 0$) at the mid-height of the FC. The downstream distance along the wake center-line from the cylinder center ($X = 0$) to the location, where the streamwise turbulence intensity (Tu_u) has a peak value, was used to define the length of the vortex formation region. It was assumed that the transverse velocity component induced on each side is negligible and that the two vortices have the same convection velocity (Bearman and Wadcock, 1973). The vortex formation length at the mid-span height of $Z/L = 0.5$ is relatively large compared with that of the 2-D cylinder, irrespective of its free-end tip shape. For the hemispherical tip, in particular, the length of the vortex formation region is shortest among the four free-end shapes tested. The streamwise turbulence intensity increases gradually with downstream distance, up to $X/D = 2.5$. Thereafter it is difficult to observe a clear peak, excluding the FC with a hemispherical tip.

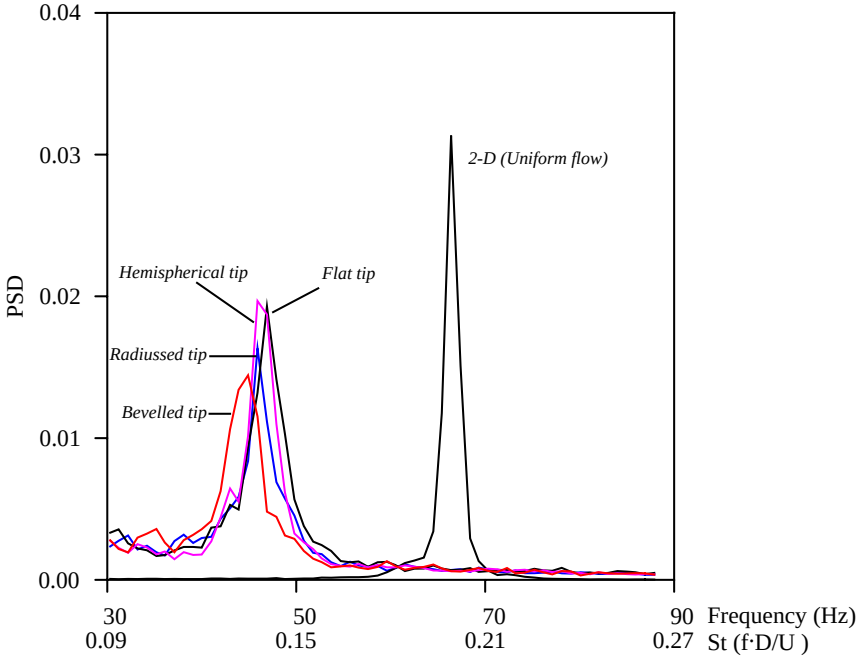

Fig. 8. Comparison of vortex shedding frequencies ($X/D = 3$, $Y/D = 2$, $Z/L = 0.5$).

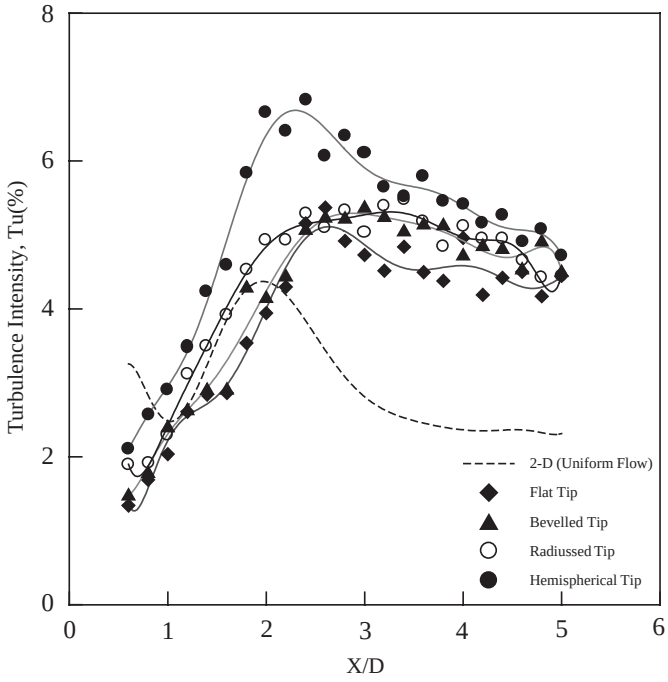

Fig. 9. Comparison of streamwise turbulence intensity ($Y/D = 0$, $Z/L = 0.5$).

3.3. Spectral analysis

Fig. 10 shows the PSD distributions of the streamwise velocity component measured along the wake center-line ($Y/D = 0$) at the height of $Z/L = 0.95$. Park and Lee (2000) found a peculiar flow structure having a 24 Hz frequency

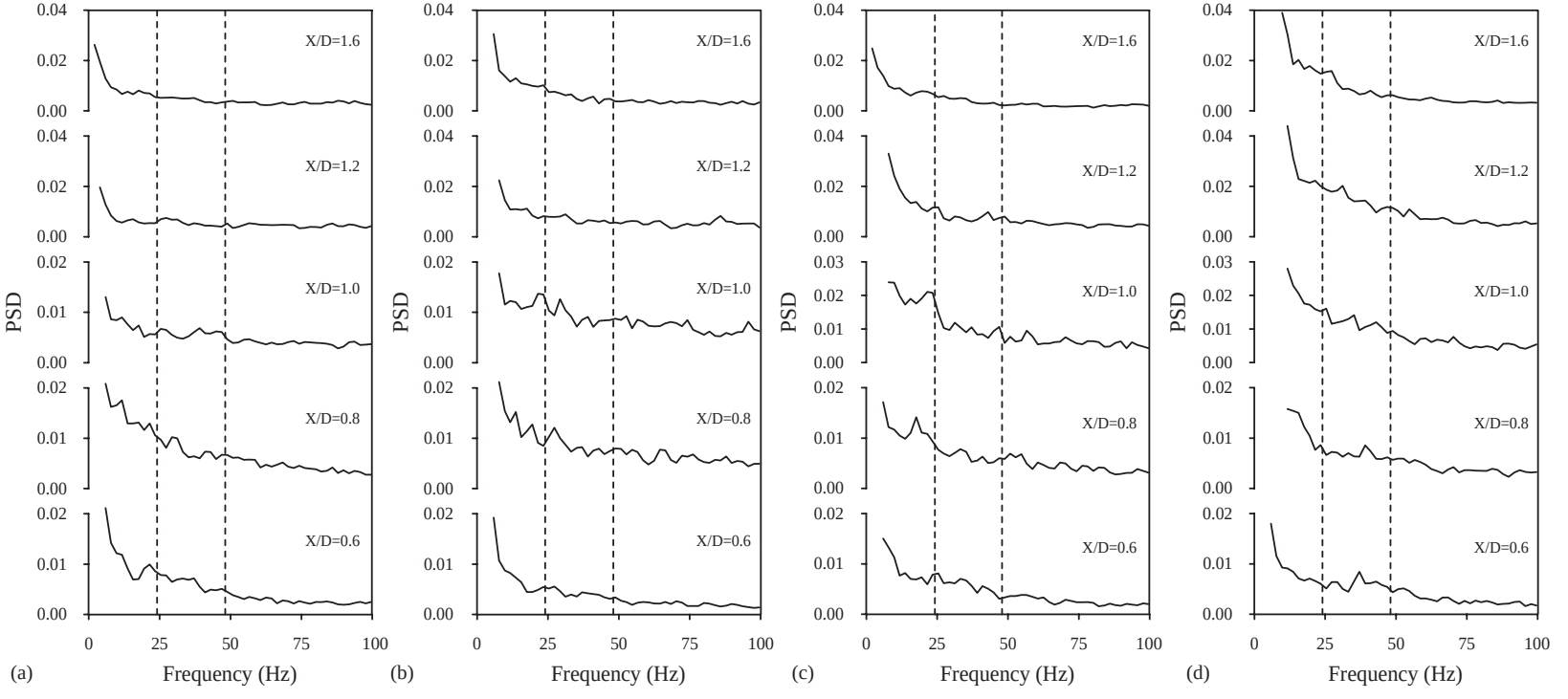

Fig. 10. Power spectral density distributions along the streamwise direction ($Y/D = 0, Z/L = 0.95$): (a) flat tip; (b) bevelled tip; (c) radiussed tip; and (d) hemispherical tip.

component near the FC free end, corresponding to the Strouhal number ($St = fD/U$) of 0.072, which was different from the periodic vortex shedding frequency. It was closely related to the counter-rotating twin-vortex generated from the FC free end, and the two vortices had no phase difference. Kitagawa et al. (1999) also mentioned that the frequency of tip-associated vortices formed around the FC free end was lower than the Kármán vortex shedding frequency.

The 24 Hz frequency component appears in the near-wake region just behind the cylinder; however, it disappears further downstream. This is attributed to the descending shear layer induced by the downwash swirling vortices from the FC free end. For the FC with the flat tip, the PSD distribution shows the 24 Hz peak at the location of $X/D = 0.6$. However, the FCs with linear and radiussed tip have the 24 Hz frequency component further downstream at $X/D = 1.0$. This indicates that the tip vortices for the FC with the streamlined cut decay slowly, compared with the flat tip right-angled FC. It is interesting to note that the hemispherical FC free end has no recognizable 24 Hz peak in the near-wake region. This may be attributed to the reduced flow separation at the top crest of the hemispherical end, as shown in Fig. 5(d).

3.4. Mean flow structure

Fig. 11 shows the mean velocity fields and contour plots of the streamwise turbulence intensity around the FC free end for the four different free-end shapes. The laser light sheet illuminates the vertical XZ-plane passing through the

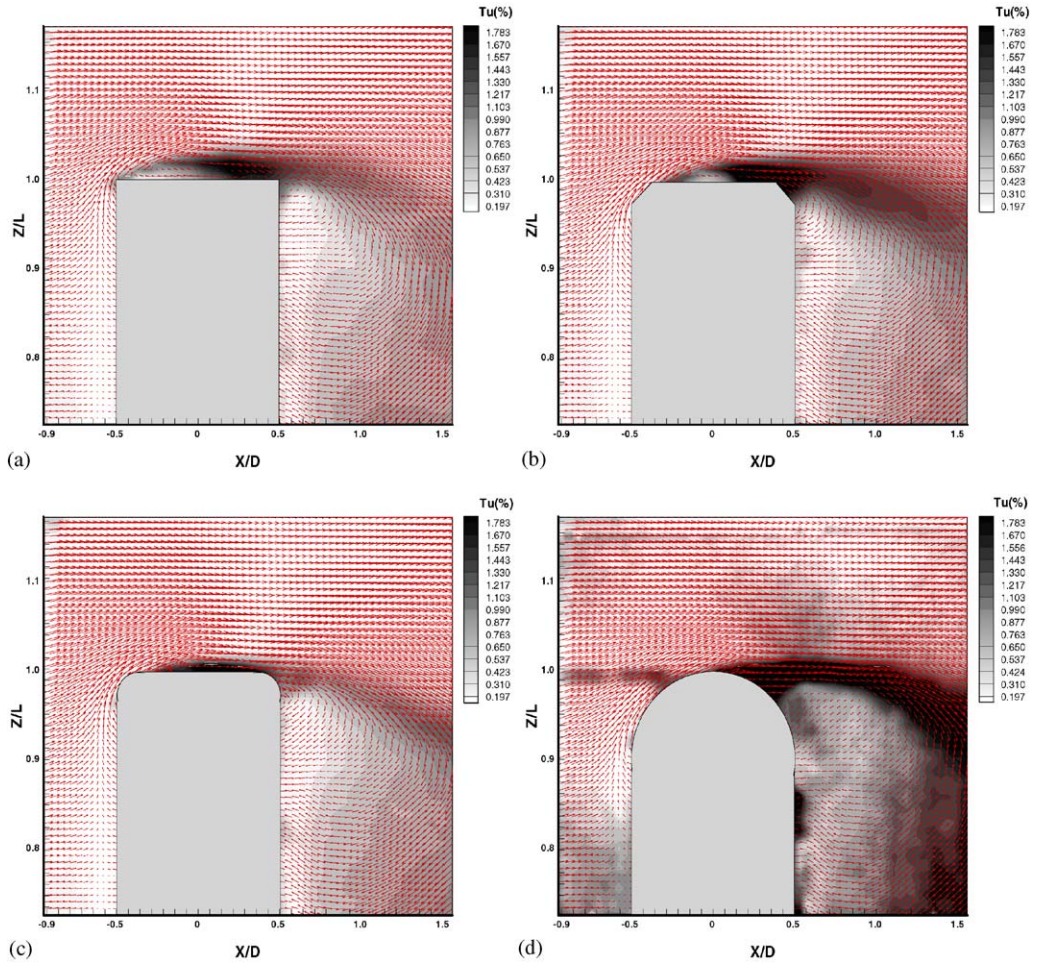

Fig. 11. Spatial distributions of mean velocity and streamwise turbulence intensity ($Y/D = 0$, XZ-plane): (a) flat tip; (b) bevelled tip; (c) radiussed tip; and (d) hemispherical tip.

wake center-line ($Y/D = 0$). The oncoming flow accelerates upward toward the forward free end and then separates from the FC free-end circumference. The streamwise turbulence intensity has relatively large values in the forehead region of the flat-tip free end. When the corner of the FC free end is cut into a smooth shape, however, the turbulence intensity at the forehead region is decreased due to the streamlined tip configuration. In the central wake plane, the separated shear layer reattaches just ahead of the downstream free end. The streamwise turbulence intensity has large values in this reattachment region. The size of the separation bubble formed above the free end of the flat-tip FC is bigger than that of the radiussed tip and the hemispherical tip.

After passing the FC free end, the separated shear layer moves downward toward the FC mid-span height and forms a large-scale recirculation flow behind the cylinder. The descending separated shear flow angle varies according to the FC free-end shape. The declining angle for the FC with the flat tip is larger than that of the streamlined edges. This explains the rapid descent of the vortex pair shown in Fig. 10. In addition, the shear layer separated from the flat-tip FC free end grows wider as it goes further downstream. For the FC with the hemispherical free end, the turbulent shear layer separated from the FC free end is thinner and has higher turbulence intensity, compared with the other three free-end shapes. On the other hand, the radiussed tip FC has the smallest streamwise turbulence intensity in the region near the FC free end.

Fig. 12 shows contour plots of TKE in the wake center plane. As expected from Fig. 11, due to dominant streamwise velocity component, the radiussed tip FC has the least TKE in the regions above and behind the FC free end. In particular, the area having large kinetic energy above the FC free end is much smaller than that of the FCs with flat tip and bevelled tip. For the FC with hemispherical tip, the separated shear layer has the largest TKE. This may result from the concentrated flow separation on the top crest of FC free end.

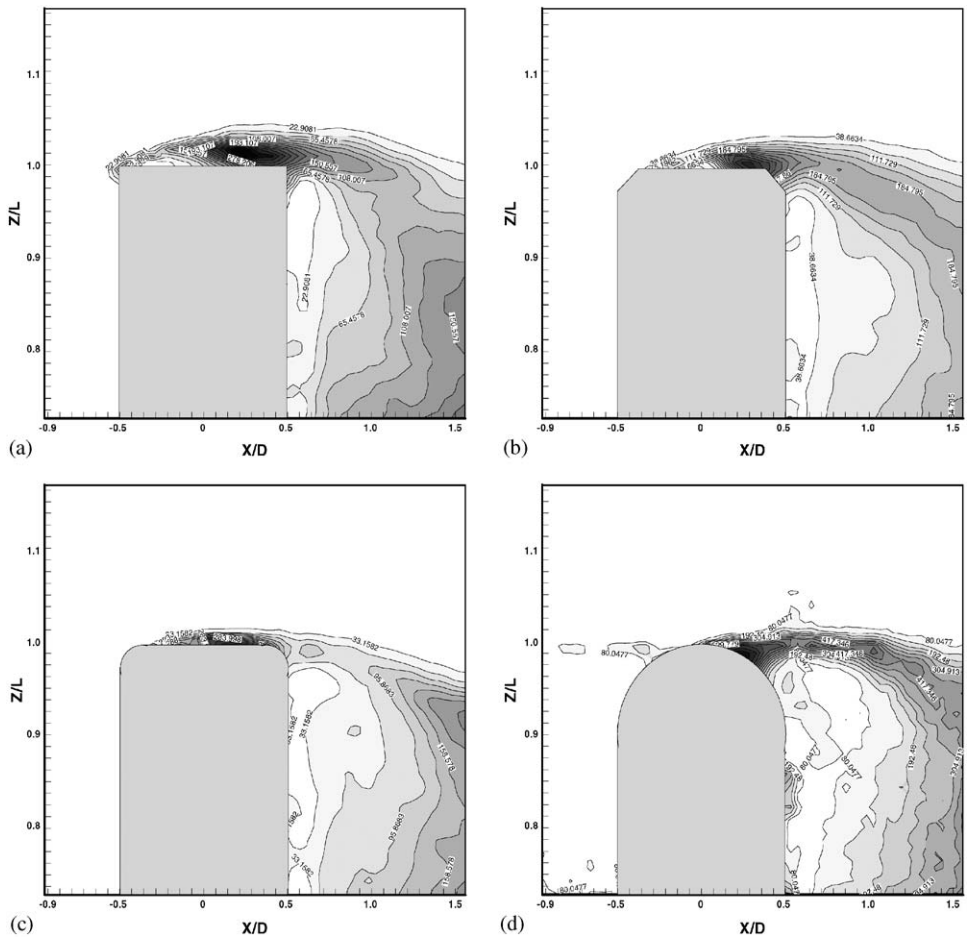

Fig. 12. Contour plots of TKE in the wake center plane ($Y/D = 0$, TKE $\times 10^2$): (a) flat tip; (b) bevelled tip; (c) radiussed tip; and (d) hemispherical tip.

The separated shear layer develops substantially as the flow moves downstream from the FC free end. The growth rate of the shear layer is usually related to the vorticity, especially to the total velocity difference ($\Delta U = U_{max} - U_{min}$) across the shear layer (Brown and Roshko, 1974). To qualitatively analyze the shear layer separated from the FC free end, we evaluated the shear layer development with respect to the FC free-end shape. The contour lines of the shear layer were depicted from the mean velocity field in the near-wake region behind the FC ($X/D \geqslant 0$). The center-line (Z_c) of the shear layer is defined as the line along which the mean velocity is ($0.67\ \Delta U + U_{min}$), where U_{min} is the minimum velocity in the separated shear layer, as is the case for the plane mixing layer (Castro and Haque, 1987).

Fig. 13 shows the center-line ($Z_c = Z_{0.67}$) and the boundaries ($Z_{0.3}$ and $Z_{0.9}$) of the separated shear layers. Here, $Z_{0.3}$, $Z_{0.67}$ and $Z_{0.9}$ indicate the lines along which U/U_{max} has the values of 0.3, 0.67 and 0.9, respectively. The Z-axis was nondimensionalized by the cylinder diameter (D) instead of the cylinder height. The center-line $Z_{0.67}$ and upper boundary $Z_{0.9}$ of the separated shear layer decreases when the corner of FC free end is cut bevelled and rounded. Especially, the upper boundary ($Z_{0.9}$) shows large variation according to the FC tip shape in the initial stage of the separated shear layer. The upper boundary for the flat tip is nearly flat and that for the linear and radiussed tip is slightly increased and decreased, respectively. However, the trajectory of $Z_{0.9}$ for the hemispherical free end is increased up to $X/D = 0.8$. This seems to result from the size of the recirculation bubble formed above the FC free end. Further downstream, the upper shear layer descends downward as the flow goes downstream irrespective of FC free-end shape. However, for the hemispherical free end, the angle of inclination of the upper shear layer is not so large. This is attributed to the fact that the separated shear layer is concentrated into a relatively small vortex tube with small loss of kinetic energy compared to the other cases.

Fig. 14 shows the mean velocity fields and contours of streamwise turbulence intensity measured at several horizontal XY planes near the right-angled FC free end. The velocity fields were obtained by moving the horizontal laser light sheet downward from $Z/L = 1.083$ to 0.872. In the region above the free end ($Z/L = 1.083$ and 1.039), the flow velocity is almost uniform except for a slight velocity fluctuation just behind the FC free end. This results from the fact that the upward movement of the oncoming flow is limited only in the region just above the FC free end. The flow reverses direction in the vicinity of the FC top surface due to the recirculation bubble formed above the FC free end.

In the region near the downstream end of the FC, we observe the descending separated shear flow in the horizontal planes of $Z/L = 1.0$ and 0.983. The shear flow separated from the backward edge of FC free end descends into the wake center with high turbulence intensity. The spatial distributions of mean velocity and streamwise turbulence intensity are nearly symmetric with respect to the central plane ($Y/D = 0$) of the wake. This is attributed to the fact that the descending shear layer from the FC free end and the entrained flow from both sides of the FC are symmetric and they

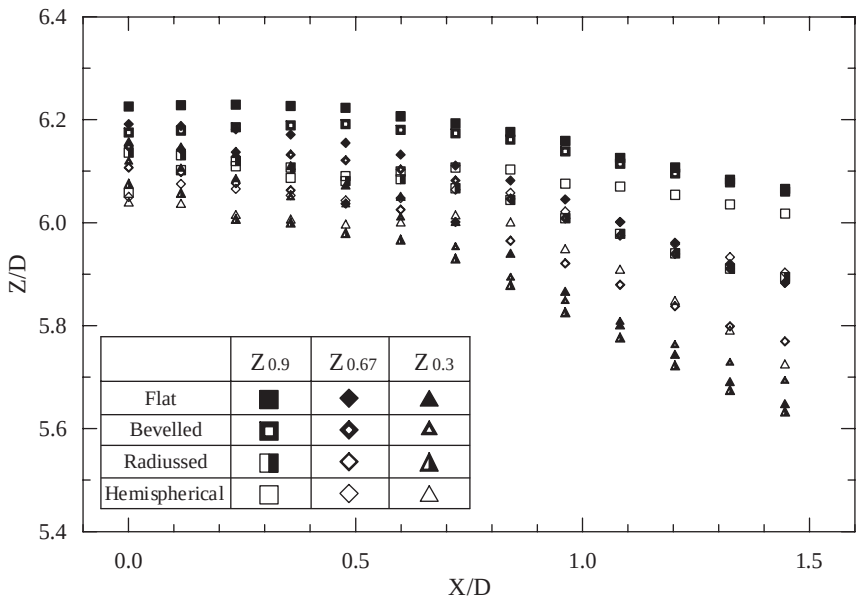

Fig. 13. Development of the separated shear layers ($X/D \geqslant 0$).

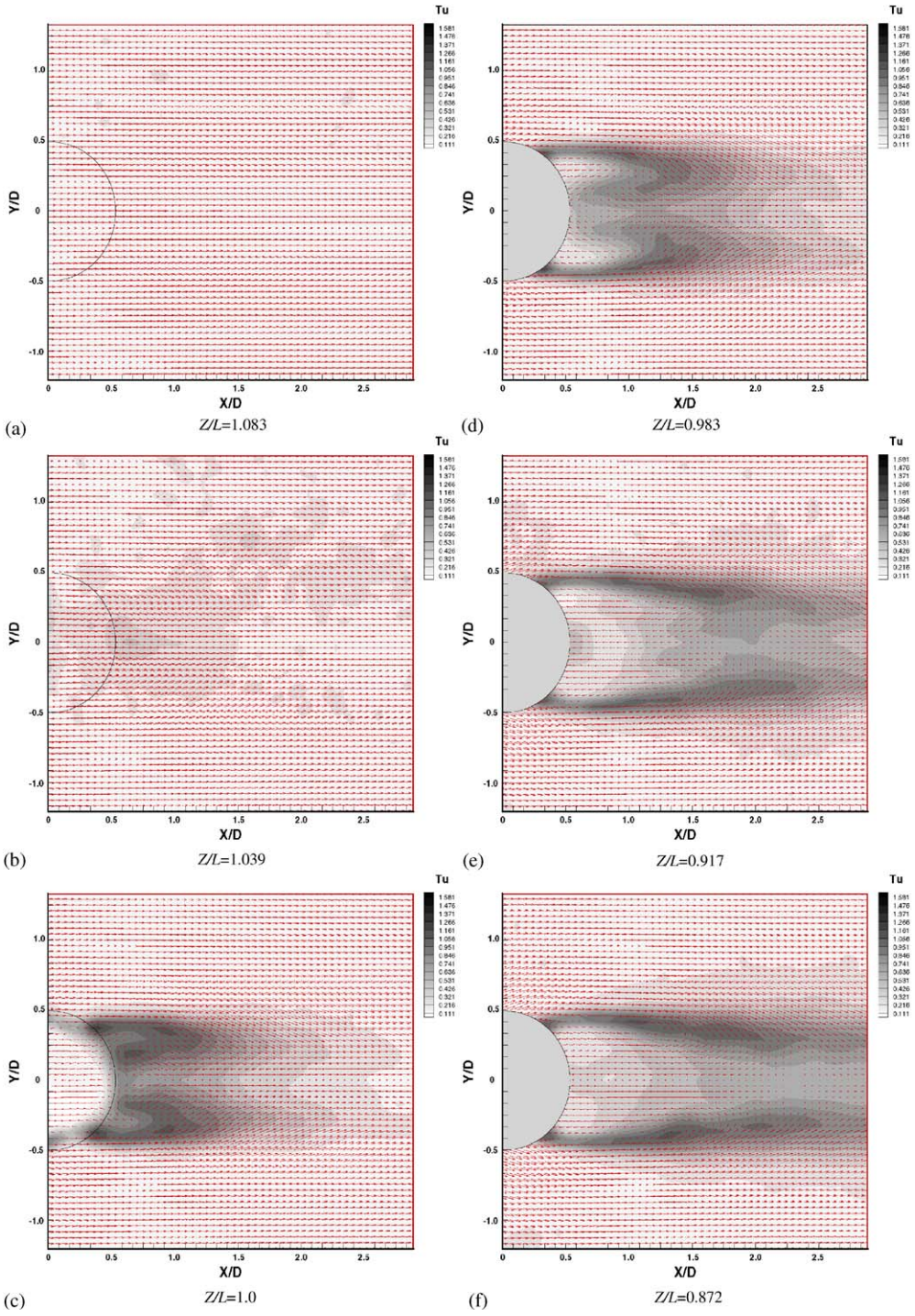

Fig. 14. Variation of mean velocity field and streamwise turbulence intensity distributions near the free end of flat tip FC (XY-plane): (a) $Z/L = 1.083$; (b) $Z/L = 1.039$; (c) $Z/L = 1.0$; (d) $Z/L = 0.983$; (e) $Z/L = 0.917$; and (f) $Z/L = 0.872$.

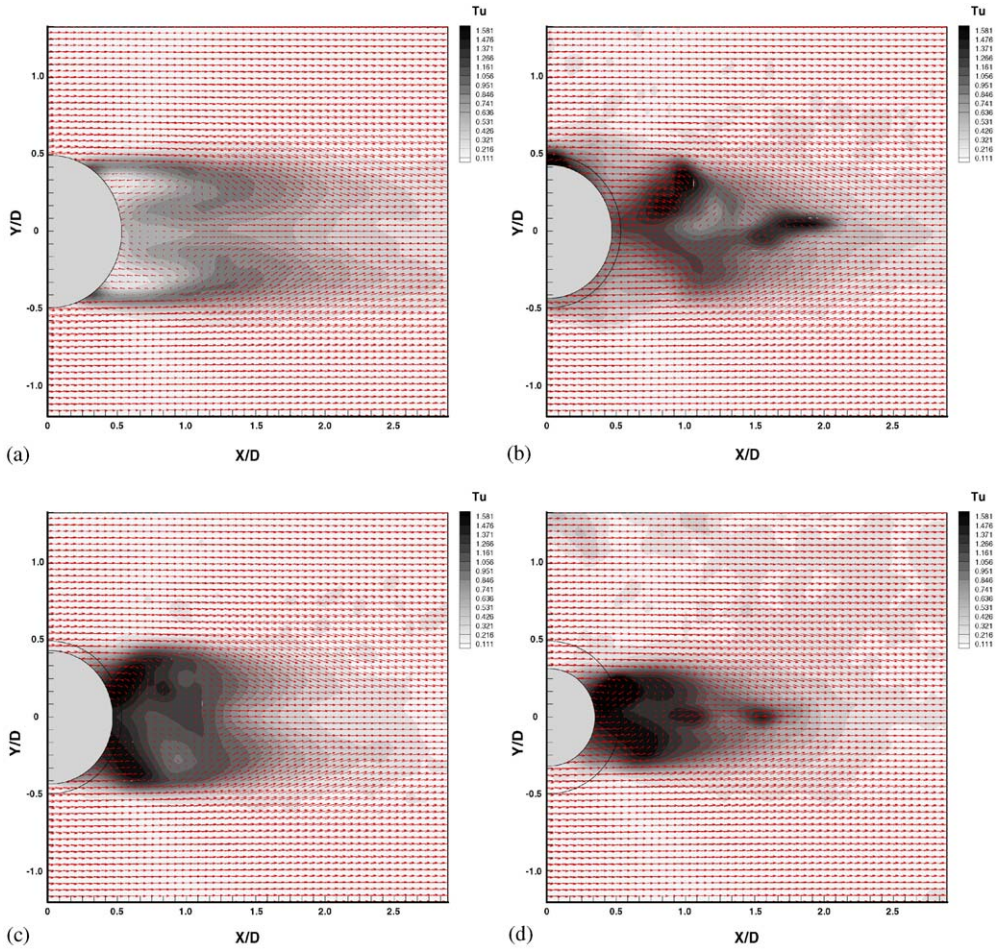

Fig. 15. Mean velocity fields and streamwise turbulence intensity distributions in the horizontal XY-plane at $Z/L = 0.983$: (a) flat tip; (b) bevelled tip; (c) radiussed tip; and (d) hemispherical tip.

interact in a symmetric manner within the near-wake region. In addition, the streamwise turbulence intensity distributions maintain the double peak shape far downstream. Traversing further down the cylinder axis, the separated shear layer from the FC free end descends further downstream as shown in Figs. 14(e) and (f).

Fig. 15 shows the mean velocity field and contours of streamwise turbulence intensity measured at a height of $Z/L = 0.983$ in the central XY-plane. The mean velocity field is nearly symmetric with respect to the wake center plane ($Y/D = 0$), irrespective of FC free-end shape. For the plain corner cut FC, the streamwise turbulence intensity distribution shows the double peak shape up to $X/D = 2.5$. For the radiussed tip FC, the separated shear flow has strong turbulence intensity in the region just behind the cylinder. This may be closely related to the small recirculation bubble formed above the FC free end. The turbulence intensity for the FC with hemispherical tip is high in the narrow separated shear layer, compared with the three other cases.

Fig. 16 shows the contour plots of spanwise vorticity (ω_z) in the horizontal XY-plane at $Z/L = 0.983$ for four different free-end shapes. In general, the entire flow field consists of two symmetric vortices with positive or negative values with respect to the wake center plane ($Y/D = 0$), irrespective of FC free-end shape. For the FC with the plain corner cut, the maximum vorticity peaks occur at $Y/D = \pm 0.4$ in the region just behind the cylinder and the spatial distribution of spanwise vorticity is elongated in the streamwise direction due to strong separated shear flow from the both sides compared with the other three cases of smoother corners. From these results, we can see that the simple corner shaping of a sharp-edged tip changes the vortex structure behind the cylinder significantly. The peak values of vorticity for the linear and radiussed tip FC is less than half of that for the flat-tip FC. The

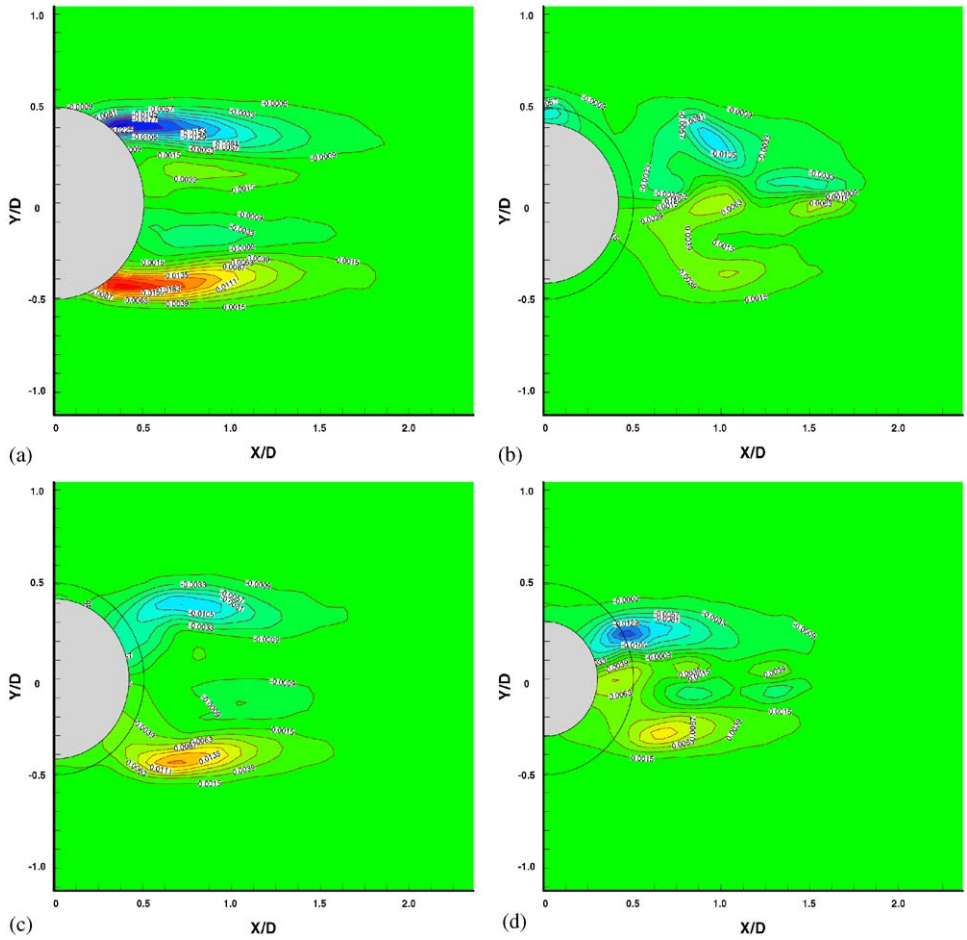

Fig. 16. Contour plots of spanwise vorticity ω_z in the horizontal XY-plane at $Z/L = 0.983$: (a) flat tip; (b) bevelled tip; (c) radiussed tip; and (d) hemispherical tip.

distance between the two vorticity peaks for the hemispherical FC is smaller than the other FC end shapes tested in this study.

4. Conclusions

The flow around a surface-mounted finite cylinder embedded in a simulated ABL has been investigated experimentally by varying the shape of the tip. The flow structure around a FC is markedly different from that of a 2-D cylinder. The 3-D wake structure seems to be induced from an interaction between the ambient fluids entrained from both sides of the cylinder and the separated shear flow descending from the FC free end.

The size of the recirculation bubble formed above the flat-tip FC tip is largely reduced by shaping the corner of the tip smoothly. The shear layer separating from the plain tip expands as the flow goes downstream, compared to the other tips tested. The turbulence intensity around the tip is also decreased as the tip is modified to a more streamlined shape.

The recirculation bubble formed above the tip and the width of the separated shear layer behind the FC is reduced. A counter-rotating longitudinal vortex pair is formed in the region just behind the square tip. These two longitudinal vortices are of similar size and are nearly symmetric with respect to the central plane of the wake. When the right-angled corner of the tip is changed to a beveled or a rounded shape, this vortical structure becomes weaker and almost disappears.

5. Summary

Many practical bluff bodies such as tall buildings can be modelled as a FC with a free end rather than an infinite cylinder. The presence of a free end changes the flow structure in the near-wake region, including the vortex shedding, vortex structure and the surface pressure distribution.

In the present study, the flow structure around the free end of a finite circular cylinder embedded in an ABL over open terrain was investigated experimentally by modifying the free-end shape. The experiments were carried out in a closed-return subsonic wind tunnel. A FC with an aspect ratio (height/diameter) of 6 was mounted vertically on a long flat plate. The velocity fields near the FC free end were measured using the single-frame double-exposure PIV method. A hot-wire anemometer was also employed to analyze the spectral characteristics of the flow structure.

For the FC with a right-angled plain cut free end, there is a peculiar vortical structure showing counter-rotating twin vortices near the FC free end. It is caused by the interaction between the entrained irrotational fluids from both sides of FC and the downwash flow from the FC free end. When the sharp corner of FC free end is rounded into a smooth shape, this vortical structure almost disappears.

Due to the descending separated shear flow from the FC free end, regular vortex shedding from the cylinder seems to be suppressed and the vortex formation region is barely distinguishable in the region near the FC free end, irrespective of the free-end edge shape. For the case of the plain cut free-end FC, the separated shear flow has stronger downwash compared with the round cut free end, reducing the recirculation bubble behind the FC.

Acknowledgements

The authors thank the supports of NRL (National Research Laboratory) program of the Ministry of Science and Technology, Korea.

References

Adrian, R.J., 1991. Particle-imaging techniques for experimental fluid mechanics. Annual Review of Fluid Mechanics 23, 261–304.

Baban, F., So, R.M.C., 1991. Aspect ratio effect on flow-induced forces on circular cylinders in a cross-flow. Experiments in Fluids 10, 313–321.

Bearman, P.W., Wadcock, A.J., 1973. The interaction between a pair of circular cylinders normal to a stream. Journal of Fluid Mechanics 61, 499–511.

Brown, G.L., Roshko, A., 1974. On density effects and large structure in turbulent mixing layers. Journal of Fluid Mechanics 64 (4), 775–816.

Castro, I.P., Haque, A., 1987. The structure of a turbulent shear layer bounding a separation region. Journal of Fluid Mechanics 179, 439–468.

Farivar, D., 1981. Turbulent uniform flow around cylinders of finite length. AIAA Journal 19 (3), 275–281.

Fox, T.A., Apelt, C.J., West, G.S., 1993. The aerodynamic disturbance caused by the free-ends of a circular cylinder immersed in a uniform flow. Journal of Wind Engineering and Industrial Aerodynamics 49, 389–400.

Kahraman, A., Sahin, B., Rockwell, D., 2002. Control of vortex formation from a vertical cylinder in shallow water: effect of localized roughness elements. Experiments in Fluids 33, 54–65.

Kareem, A., Cheng, C.M., 1999. Pressure and force fluctuations on isolated roughened circular cylinders of finite length in boundary layer flows. Journal of Fluids and Structures 13, 907–933.

Kitagawa, T., Fujino, Y., Kimura, K., 1999. Effects of free-end condition on end-cell-induced vibration. Journal of Fluids and Structures 13, 499–518.

Okamoto, S., Sunabashiri, Y., 1992. Vortex shedding from a circular cylinder of finite length placed on a ground plane. Journal of Fluids Engineering 114, 512–521.

Park, C.W., Lee, S.J., 2000. Free-end effects on the near wake flow structure behind a finite circular cylinder. Journal of Wind Engineering and Industrial Aerodynamics 88, 231–246.

Park, C.W., Lee, S.J., 2002. Flow structure around a finite circular cylinder embedded in various atmospheric boundary layers. Fluid Dynamics Research 30 (4), 197–215.

Shin, D.S., Choi, J., Lee, S.J., 2000. Velocity field measurements of flow inside snout of continuous hot-dip galvanizing process using a single-frame PIV technique. Iron and Steel Institute of Japan International 40 (5), 484–490.

Simiu, E., Scanlan, R.H., 1996. Wind Effects on Structures. Wiley, New York, pp. 46–64.

Slaouti, A., Gerrard, J.H., 1981. An experimental investigation of the end effects on the wake of a circular cylinder towed through water at low Reynolds numbers. Journal of Fluid Mechanics 112, 297–314.

Szepessy, S., Bearman, P.W., 1992. Aspect ratio and end plate effects on vortex shedding from a circular cylinder. Journal of Fluid Mechanics 234, 191–217.

Uematsu, Y., Yamada, M., Ishii, K., 1990. Some effects of free-stream turbulence on the flow past a cantilevered circular cylinder. Journal of Wind Engineering and Industrial Aerodynamics 33, 43–52.

West, G.S., Apelt, C.J., 1982. The effects of tunnel blockage and aspect ratio on the mean flow past a circular cylinder with Reynolds numbers between 10^4 and 10^5. Journal of Fluid Mechanics 114, 361–377.

Williamson, C.H.K., 1989. Oblique and parallel modes of vortex shedding in the wake of a circular cylinder at low Reynolds numbers. Journal of Fluid Mechanics 206, 579–627.